UNIVERSITÀ DEGLI STUDI DI PADOVA

Dipartimento di Fisica e Astronomia "Galileo Galilei"

Corso di Laurea in Fisica

Tesi di Laurea

Optimal Control of two-level quantum systems via Chopped RAndom Basis algorithm

Relatore

Prof. Simone Montangero

Laureando

Luna Cesari

Anno Accademico 2019/2020

Abstract

This work is devoted to the study and the application of the Chopped RAndom Basis (CRAB) control algorithm as an efficient, versatile optimal control technique to be used for the purpose of enhancing the quality of quantum processes. In order to show its principal aspects, the method is here applied to different systems, in particular one-qubit and two-qubit system. Finally, the dressed CRAB algorithm is presented as a valid alternative to the standard method, as it comes with the additional property of guaranteed convergence to the global optimum.

Contents

Introduction

Optimal Control Theory (OCT) is an outcome of the calculus of variations, dealing with the identification of a feasible scheme, policy, program, strategy, or campaign, in order to achieve the optimal outcome of a system, so as to minimize a certain cost or, equivalently, to maximize a certain profit [18].
Its history dates back to hundreds of years: in 1696, Johann Bernoulli's brachistochrone curve problem was one of the earliest examples of the field. Many other mathematicians were involved and an important step in the development of the theory was the formulation of the Pontryagin's maximum Principle by L. S. Pontryagin, providing the necessary conditions for (constrained) optimal control [36]. Today, OCT is a mature mathematical discipline, with numerous applications in both science and engineering.
Likewise, Quantum Optimal Control Theory (QOCT) is concerned with active manipulation of physical and chemical processes on the atomic and molecular scale. The first important step was taken in the late 1980s, with great progresses following in the last three decades: from its early applications in the design of electromagnetic field profiles [36], many sophisticated QOC techniques has been introduced, such as Krotov [17] or GRAPE (GRadient Ascent Pulse Engineering)[16] methods, whose examples of recent applications are superconducting circuits [22], ion traps [21], molecular dynamics [33], and nuclear magnetic resonance (NMR) [15, 35]. The development of QOCT is based on many converging theoretical progresses, such as mathematical control theory or numerical mathematics, and technological advances, in particular some crucial ones, as intense femtosecond laser sources and pulse shapers [18].
Nowadays, this theory contributes to quantum engineering, e.g., allowing coherence and open system control, as well as quantum information, providing practical means to explore decoherence-free subspaces or other noise-avoiding strategies [12, 1]. QOCT provides recipes to achieve quantum operations with high accuracy and speed, succeeding where other techniques fail, such as adiabatic quantum control: indeed, adiabatic protocols require long-duration fields, making the quantum process prone to decoherence or noise effects induced by the unavoidable interaction with the external environment [36].
However, some limitations can occur in the application of QOC procedure, such as the need for an accurate knowledge of the system in order to estimate the optimal fields or the incompatibility between the level of tunability required for the driving fields and the existing experimental means. Moreover, since standard OC algorithms compute the optimal control fields by solving a set of Euler-Lagrange equations, it turns out that the equation for the correction to the driving field is highly dependent on the choice of the cost function and on the constraints the system is subjected to, making these methods less versatile.
In this contest, the CRAB (Chopped RAndom Basis) algorithm has been introduced as a possible solution to the aforementioned problems [5, 30]. More precisely, it consists of the truncation and randomization of the function basis chosen to parametrize the time-dependent control fields that drive the evolution of the system. Therefore, the problem is recast into a functional minimization with respect to the parameters that define the Hamiltonian and the target state. The extremization of the multivariable function is then numerically realized by proper approaches, such as

direct search methods. Examples of important current applications of the CRAB algorithm are the autonomous calibration of electron spin, quantum operations in diamond [10], state engineering of Bose-Einstein condensates [14], and entanglement creation and manipulation with Rydberg atoms [28].
This thesis intends to analyze this algorithm, presenting advantages and possible applications.

Theory

The theoretical framework of OC is presented in this chapter. First, an insight into the theory of quantum optimal control is reported, along with its main concepts; second, the CRAB algorithm is described as a numerical method applied to solve QOC problems.

1.1 Quantum Optimal Control Theory

An optimal control problem is formulated in terms of searching for the best control laws in order to drive the evolution of a system in a fixed time T, so that a cost functional J is extremized. We focus on systems whose dynamics is described by the Schrödinger equation [1] and whose controls consist of a set of time-dependent driving fields $\vec{\gamma}(t) = (\gamma_1(t), \gamma_2(t), ..., \gamma_m(t))$, so that

$$\imath \frac{d}{dt} |\psi(t)\rangle = H(\vec{\gamma}(t)) |\psi(t)\rangle \tag{1.1}$$

Typically, the Hamiltonian considered in QOC problems is $H(\vec{\gamma}(t)) = H_d + \vec{\gamma}(t) H_c$, where H_d and H_c are the drift and control Hamiltonian respectively. Generally, the space the set of the control fields belongs to is the space of locally bounded, sufficiently smooth, square integrable functions of time defined on some interval [0, T], with T fixed [3]. We focus on finite-level quantum systems, so that the Hilbert space the Hamiltonian acts on is $\mathcal{H} = \mathbb{C}^N$. Moreover, we consider pure states: mixed states can be included and controlled, but they fall beyond the scope of this thesis. The cost functional is typically expressed as

$$J(\vec{\gamma}, T) = F(\psi_{\vec{\gamma}}(T), T) + \int_0^T L(t, \psi_{\vec{\gamma}}(t), \vec{\gamma}(t)) dt \tag{1.2}$$

where the end cost term $F(\psi_{\vec{\gamma}}(T), T)$, called Mayer term, usually yields the distance between the final evolution state according to the Schrödinger equation $\psi_{\vec{\gamma}}(T)$ and a goal state ψ_G in some metric, while the second term, the Lagrange term, adds up running costs $L(t, \psi_{\vec{\gamma}}(t), \vec{\gamma}(t))$ over the whole time interval of the process. Generally, the representation of Eq. (1.2) is referenced as Bolza form [36].
More specifically, three types of problems corresponding to different choices of F are the most commonly studied: evolution-operator control, state control and observable control.
In evolution-operator control, the objective is to generate $U_{\vec{\gamma}}(T)$ so that the distance to the target unitary transformation W is minimized, therefore $F_1 = 1 - \left\| U_{\vec{\gamma}}(T) - W \right\|^2$. A common choice for the normalized matrix norm $\|\cdot\|$ is the squared Hilbert–Schmidt norm with an appropriate normalization [2], so that the Mayer-type cost functional results

$$F_1 = \frac{1}{N} Re \left\{ Tr[W^\dagger U_{\vec{\gamma}}(T)] \right\} \tag{1.3}$$

[1] Hereafter, reduced Planck constant is set to $\hbar = 1$.
[2] $\|\cdot\| = \frac{1}{2N} Re \left\{ Tr[X^\dagger X] \right\}$, where N is the size of the basis.

On the other hand, the aim for state control problems is to generate a final state $\left|\psi_{\vec{\gamma}}(T)\right\rangle$ so that it is as close as possible to the target one $|\psi_G\rangle$. Therefore, the Mayer term typically is

$$F_2 = 1 - |\left\langle\psi_G\right|\left.\psi_{\vec{\gamma}}(T)\right\rangle|^2 \tag{1.4}$$

Finally, observable control goal consists of extremizing the expectation value of a target quantum observable, that might either be evaluated at the final time T, e.g. Eq. (1.5), or averaged over the whole time interval $[0, T]$, as in Eq. (1.6)

$$F_3 = \left\langle\psi_{\vec{\gamma}}(T)\right| O \left|\psi_{\vec{\gamma}}(T)\right\rangle \tag{1.5}$$

$$F_4 = \frac{1}{T}\int_0^T \left\langle\psi_{\vec{\gamma}}(t)\right| O \left|\psi_{\vec{\gamma}}(t)\right\rangle dt \tag{1.6}$$

It is also possible to include additional constraints on the pulse or accessible states, such as maximum pulse amplitude, maximum bandwidth of the pulse or highest populated energy.
Generally, the necessary condition for a solution of the extremization problem subject to the dynamical constraint expressed in Eq. (1.1) is that the first-order functional derivatives of J with respect to $\psi_{\vec{\gamma}}$, $U_{\vec{\gamma}}$ and $\vec{\gamma}$ are equal to zero [30]. As a result, optimal controls can be obtained by solving the corresponding Euler–Lagrange equations. Usually, such problems are nonlinear and therefore do not have analytic solutions, so it is necessary to employ numerical methods whose main examples could be categorized in direct search methods, indirect search methods, function expansion methods and miscellaneous methods [3].
The main characteristics of QOCT are listed in the following paragraphs.

1.1.1 Controllability

A system is said to be controllable if for any pair of configurations $\zeta_1, \zeta_2 \in \Gamma$ there exists a set of time-dependent control $\vec{\gamma}(t)$ that can drive the system from the initial configuration ζ_1 to the final one ζ_2 in a finite time T, where $\Gamma = \{\zeta\}$ is the set of configurations. Here, the notion of configuration refers to the state of the system, the expectation value of an observable or the evolution operator U, depending on the specific control problem. For an N-level closed system, it has been demonstrated [31, 2], that a necessary and sufficient condition for evolution-operator controllability (that is equivalent to state controllability) is that the the Lie group generated by the system's Hamiltonian is U(N) (or SU(N) for a traceless Hamiltonian) [3]. Nevertheless, even if a system is controllable, finding the optimal driving field could be arbitrary difficult. On the contrary, it might still be possible to identify a specific transformation after a given time although a system is not controllable. Indeed, the controllability criterion states that any transformation is possible [36].

1.1.2 Quantum speed limit

This limit refers to an energy-time uncertainty relation. As theoretical esteem, there exist two independent relations that define the minimal time needed for a system to evolute from an initial state to an orthogonal one: the Mandelstam-Tamm bound [23]

$\tau_{QSL} = \frac{\pi\hbar}{2\Delta E}$ and Margolus-Levitin bound [24] $\tau_{QSL} = \frac{\pi\hbar}{2E}$, where $E = \langle\psi_0| H |\psi_0\rangle$ and $\Delta E = \sqrt{\langle\psi_0| (H-E)^2 |\psi_0\rangle}$, so a possible definition of the minimal evolution time is [36]

$$\tau_{QSL} \geq max \left\{ \frac{\pi\hbar}{2\Delta E}, \frac{\pi\hbar}{2E} \right\} \tag{1.7}$$

Otherwise, an experimental bound could be provided by analyzing the esteem of the cost functional resulting from the optimization process as a function of T and proving that the objective functional reaches values arbitrarily close to the desired ones only when T is fixed above a certain threshold τ_{QSL} [7].
Anyway, these relations shows that there exist a fundamental bound in the time needed for a quantum system to evolve in its Hilbert space which is not attributed to numerical or experimental limits nor our lack in finding a better solution.

1.1.3 Field information

The dimension of a quantum OC problem is defined by the minimal number of independent degrees of freedom D in the OC field necessary to achieve the desired transformation up to precision ϵ, that could be the minimal number of sampling points n_s, of the frequencies in the control field, or the dimension of the subspace of functions the control field has nonzero projection on [20]. It has been demonstrated that the number of independent degrees of freedom in the pulse scales only polynomially with the dimension of the set of time-polynomial reachable states from an initial state [36]. These theorems show how the information content of typical quantum optimal control problems is very limited.

1.1.4 Landscape

The control landscape is defined as

$$J(\vec{\gamma}) = F(\left|\psi_{\vec{\gamma}}(T)\right\rangle) \tag{1.8}$$

that is a function of the final state $\left|\psi_{\vec{\gamma}}(T)\right\rangle$ or, equivalently, a functional of the set of control fields $\vec{\gamma}(t)$. The topology of the control landscape, that is the character of its critical points, including local and global extrema, determines whether local search algorithms will converge to globally optimal solutions to the control problem or it will get stuck in the so called traps, that is local optimal solutions. It has been shown that, for controllable systems with no constraint on the pulse, all known traps only occur for constant control fields [9, 29]. Therefore, it is commonly accepted that unconstrained control landscapes for all practical purposes have no traps. A more detailed analysis is presented in section 3.1.

1.2 Chopped random basis algorithm

The idea behind the CRAB algorithm is to expand the control fields γ_j in a function basis $f_i(t)_{i=1,\ldots,N_c}$ that is truncated to a finite number N_c of elements, which are

usually picked from an orthonormal basis and then randomized:

$$\gamma_j(t) = \sum_{i=1}^{N_c} c_j^i f_j^i(\omega_j^i, r_j^i, t) \tag{1.9}$$

where $\vec{\omega}_j$ are parameters the function basis depends on and $\vec{r}_j$ are random numbers. As a consequence, the orthonormalization of the basis is broken, but the effective search volume in terms of the function space is enlarged, enhancing the algorithm convergence while keeping constant the number of optimization parameters.
The optimization is performed by starting from an initial pulse guess $\gamma_j^0(t)$ and then looking for the best correction as shown in the following:

$$\gamma_j^{CRAB}(t) = \xi_j^+ \gamma_j^0(t) + [1 + \xi_j^{\mathrm{x}}(\gamma_j^0(t) - 1)]\gamma_j(t) \tag{1.10}$$

where the two binaries $\xi_j^+, \xi_j^{\mathrm{x}} \in \{0, 1\}$ set how the correction should be applied on the initial guess. The most common choices are $(\xi_j^+, \xi_j^{\mathrm{x}}) = (1, 0)$ and $(\xi_j^+, \xi_j^{\mathrm{x}}) = (1, 1)$. For the option $(\xi_j^+, \xi_j^{\mathrm{x}}) = (1, 0)$ the algorithm is not able to shift or remove any of the roots that $\gamma_j^0(t)$ might exhibit [36].
The choice of the function basis could be completely arbitrary, unless there exists a physical motivation behind it. For example, if the experimental apparatus poses bandwidth constraints, the Fourier basis with respective limited highest frequency proportional to N_c can be selected [10]. Other possible bases are Hermite, Lagrange polynomials, or Gaussian bell curve.
The optimization consists in the extremization of the multivariable cost function $J(T, \vec{c}_j)$, which can be numerically approached with any suitable method, as gradient methods (e.g. steepest descent, conjugate gradient) or direct search methods [32]. The success of gradient methods to find global solutions in quantum control problems [8] is largely due to the fact that local minima are very rare in the control landscapes of a large class of systems, as mentioned in Sec. 1.1.4 previously. However, the numerical computation of the gradient of the control objective might be quite inefficient and, in an increasing number of interesting applications, the control objective does not allow for an analytical calculation of the gradient [6]. Moreover, CRAB optimization does not necessarily fulfill the condition of rare local minima in the optimization process anyway, as the restriction of the search basis to N_c dimensions leads to the formation of the so-called false traps [30]. For instance, usually CRAB optimal control algorithm operates by means of gradient-free minimization, directly evaluating the cost functional in carefully selected points. A particularly prevalent example in QOC is the Nelder- Mead algorithm [11, 27].
The reason why reduced-basis methods are mathematically consistent is based on the fact that quantum optimal control problems have a limited information content, as reported in the paragraph 1.1.3 of the previous section. In other words, the high-quality solutions often lie in some lower dimensional subspace of the full control space, so a proper low dimensional parametrization of the control space can a priori steer the optimization in the correct direction.

Applications

Few examples of possible applications of the CRAB method are presented in the following sections. In this context, several particular choices for the construction of the algorithm are made: a single control field expanded in the Fourier basis is considered, with the binary coefficients in Eq. (1.10) set as $\xi_j^+ = 0$ and $\xi_j^{\mathrm{X}} = 1$, hence

$$\gamma^{CRAB}(t) = \sum_{i=1}^{N_c} (A_i cos(\omega_i t) + B_i sen(\omega_i t)) \tag{2.1}$$

where $\{A_i, B_i\}_{i=1}^{N_c}$ are the parameters the optimization refers to, while the frequencies ω_i are generally fixed to relevant values if there is some physical information available, otherwise they are randomized either in a whole interval, such as in Eq. (2.2), or around the principal harmonics in Eq. (2.3), with r_i and c_i random numbers with flat distribution in the respective intervals.

$$\omega_i = \frac{2\pi r_i}{T} \quad r_i \in [r_{min}, r_{max}] \tag{2.2}$$

$$\omega_i = \frac{2\pi i(1+c_i)}{T} \quad c_i \in [c_{min}, c_{max}] \tag{2.3}$$

The cost function to be minimized corresponds here to the infidelity F_2 (see Eq. (1.4)), eventually summed to a constraint on the power of the control field (as reported in the paragraph 2.1.1)

$$J(T, \vec{A}, \vec{B}) = 1 - \left| \left\langle \psi_G \middle| \psi_{\vec{\gamma}}(T, \vec{A}, \vec{B}) \right\rangle \right|^2 \tag{2.4}$$

where $\left|\psi_{\vec{\gamma}}\right\rangle$ is computed through Runge Kutta method, while J is minimized using the Nelder-Mead method.

Nelder-Mead method This algorithm belongs to the class of direct search methods, since it uses only function values at some points in $\mathbb{R}^n$ and does not try to compute the gradient at any of these points. Since it is simplex-based, it iteratively creates a sequence of simpleces [1] to approximate an optimal point of the function to be minimized. The choice of the initial simplex depends on the nature of the problem but, generally, a too small starting simplex can lead to a local search and, consequently, the algorithm might get stuck. Therefore, a possible choice is a nondegenerate simplex [19]: it is made by generating points with a fixed step along each dimension starting from an initial one x_0, which in the following examples is set equal to the origin. At each iteration, the vertices $\{x_j\}_{j=1}^{n+1}$ of the current simplex are ordered according to the objective function values $J(x_1) \leq J(x_2) \leq ... \leq J(x_{n+1})$, where x_1 is referred to as the best vertex, and to x_{n+1} as the worst vertex. Then, a new working simplex from the current one is computed and a sequence of transformations, reflection, expansion and contraction, is performed, in order to replace only

[1] A simplex is a geometric figure in n dimensions that is the convex hull of n + 1 vertices.

the worst vertex with a better point. If this succeeds, the accepted point becomes the new vertex of the working simplex and at most two new points have been computed. If this fails, the simplex shrink towards the best vertex so that, in this case, n new vertices are computed. Therefore the Nelder-Mead algorithm typically requires only one or two function evaluations at each step (the shrink transformation rarely appears in practice [11]), while most search methods use n or even more function evaluations.
The iterative cycle is then stopped when a given number of iterations is exceeded, the simplex reaches some minimum size limit or the current best solution reaches an acceptable limit. These values are here fixed to 2000 maximum number of iterations and the absolute tolerance between iterations for the vertices and function evaluations is set equal to 10^{-3} , in other words, the iterations stop when the value of the vertices or the current best solution in consecutive steps are equal up to the third decimal place.

2.1 One-qubit optimization

Let's consider a single qubit evolution from an initial state $|\psi_0\rangle = |0\rangle$ to a target one $|\psi_G\rangle = \frac{1}{2}(|0\rangle + |1\rangle)$ [2] driven by the Hamiltonian [3]

$$H = \hat{\sigma}_z + \hat{\sigma}_x \gamma^{CRAB}(t) \tag{2.5}$$

In the following examples, the total evolution time is fixed to $T = \pi$, the total number of frequencies is set to $N_c = 2$ and the frequencies are chosen randomly as stated in Eq. (2.2), where r_i is a random number with flat distribution in $[0, 2]$. The choice of such interval is led by many tests carried out in order to identify the range of the optimal frequencies for the analyzed system.
The infidelity evaluation at the end of each iteration of the Nelder-Mead algorithm is shown in Fig. 2.1: specifically, the dashed line represents the mean value $\langle J_{Iter} \rangle$ of the infidelity over 30 different runs of the CRAB algorithm, that means thirty different sets of random frequencies and initial simpleces, while the coloured space represents the cost function oscillations between the maximum and minim value per each iteration number over the several runs.
The control field as a function of time $t \in [0, \pi]$, related to the minimization that provides the lower optimized infidelity value among the 30 iterations, is presented in Fig. 2.2.

2.1.1 Control pulse amplitude

Bounds on the control pulse amplitude frequently occurs in the practice due to experimental limitations. This could be taken into account in many different ways. Let's say b_l and b_u are the upper and the lower bound respectively, so that $b_l \leq \gamma(t) \leq b_u \quad \forall t \in [0, \pi]$. In the following examples, $b_l = -1$ and $b_u = 1$.

[2] $|0\rangle = \binom{1}{0}, |1\rangle = \binom{0}{1}$ is the computational basis in $\mathcal{H} = \mathbb{C}^2$.
[3] $\hat{\sigma}_x = \begin{pmatrix} 0 & 1 \\ 1 & 0 \end{pmatrix}$, $\hat{\sigma}_y = \begin{pmatrix} 0 & -\imath \\ \imath & 0 \end{pmatrix}$ and $\hat{\sigma}_x = \begin{pmatrix} 1 & 0 \\ 0 & -1 \end{pmatrix}$ are the Pauli's matrices.

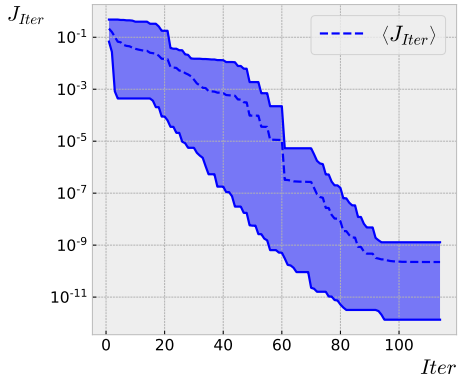

Figure 2.1: cost function (infidelity) evaluation per iteration for one-qubit system, where the number of frequencies is fixed to $N_c = 2$; the dashed line corresponds to the mean value over 30 runs of the algorithm and the coloured space shows the maximum and minimum variation of the function along the repetitions.

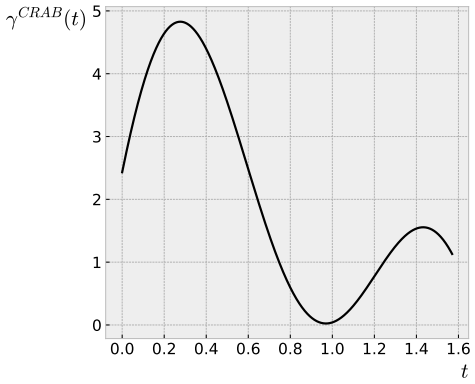

Figure 2.2: control field corresponding to the lower infidelity esteem provided among 30 repetitions of the algorithm for one-qubit system; the number of frequencies is set equal to $N_c = 2$;

A possible approach is to cut any excursion beyond b_l or b_u to the respective limit, as shown in Fig. 2.3.

$$\gamma_{cut}^{CRAB}(t) = \begin{cases} \gamma^{CRAB}(t) & \text{if} \quad b_l \leq \gamma^{CRAB}(t) \leq b_u \\ b_l & \text{if} \quad \gamma^{CRAB}(t) < b_l \\ b_u & \text{if} \quad \gamma^{CRAB}(t) > b_u \end{cases} \qquad \forall t \in [0, \pi] \tag{2.6}$$

However, this method often introduces high frequencies in the pulse due to the emerging edges [36]. Therefore, usually the limited pulse is obtained from the unconstrained one $\gamma^{CRAB}(t)$ by choosing a smooth function $\phi(\cdot)$, such as $tanh(\cdot)$, that maps $\mathbb{R} \to [-1, 1]$ and computing

$$\gamma_{shrink}^{CRAB} = \left(\frac{b_l + b_u}{2}\right) + \left(\frac{b_l - b_u}{2}\right) \phi\left(\gamma^{CRAB}(t)\right) \tag{2.7}$$

The cost function and optimized field are presented in Fig. 2.5 and Fig. 2.6.
Another possible way for the pulse amplitude to be controlled is to introduce a constraint on the power of the driving field in the cost function, so that

$$J = (1 - |\left\langle \psi_G \middle| \psi_{\vec{\gamma}}(T) \right\rangle|^2) + \beta \int_0^T |\gamma(t)|^2 \, dt \tag{2.8}$$

where β is a parameter that expresses the weigh of the constraint on the cost function. In the following example, it is fixed to 0.1, since, in this context, it results the right value to make the infidelity be equal to zero within the error (see Fig. 2.7) and also to reduce the field amplitude between $b_l = -1$ and $b_u = 1$ (see Fig. 2.8).
However, the introduction of such amplitude constraints "decreases" the search volume in terms of the function space, which means that less possible solutions are explored and the success of the algorithm is affected, as the figures 2.3, 2.5 and 2.7 show with respect to figure 2.1.

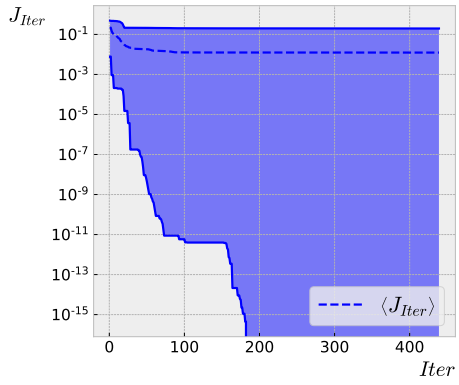

Figure 2.3: cost function (infidelity) evaluation per iteration (see caption of Fig. 2.1) estimated through a field whose amplitude has been cut between $b_l = -1$ and $b_u = 1$.

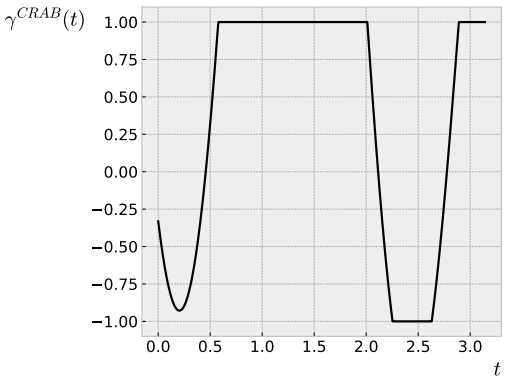

Figure 2.4: control field with cut amplitude between $b_l = -1$ and $b_u = 1$ that provides the lower infidelity esteem (see caption of FIg. 2.2).

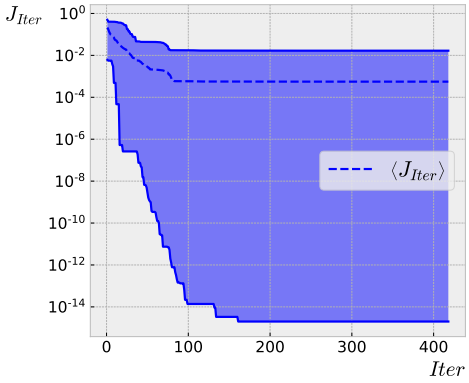

Figure 2.5: cost function (infidelity) evaluation per iteration (see caption of Fig. 2.1) estimated through a field that has been shrunk so that its amplitude is constrained between $b_l = -1$ and $b_u = 1$.

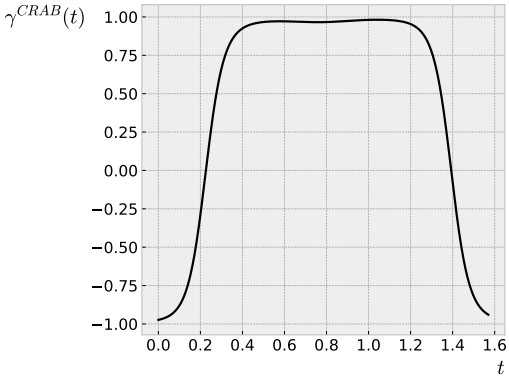

Figure 2.6: control field shrunk between $b_l = -1$ and $b_u = 1$ that provides the lower infidelity esteem (see caption of Fig. 2.2).

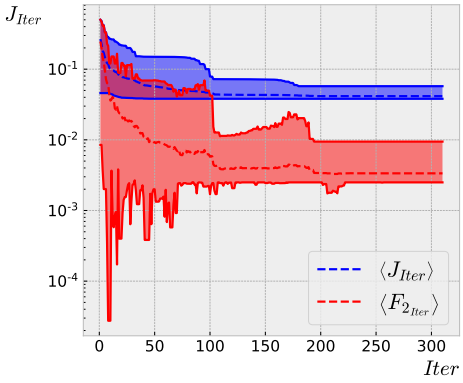

Figure 2.7: cost function (blue) and infidelity (red) evaluation per iteration (see caption of Fig. 2.1), where the cost function consists of the sum of the infidelity and a field amplitude constraint.

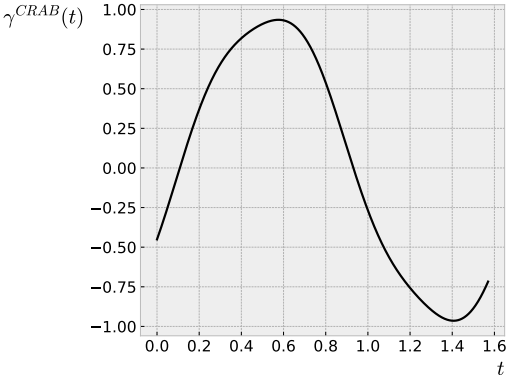

Figure 2.8: control field corresponding the lower infidelity esteem (see caption of Fig. 2.2) obtained by minimizing the Eq. (2.8), so that its amplitude results confined in $b_l = -1$ and $b_u = 1$.

2.1.2 Function basis

The choice of the function basis is arbitrary, as stated at the beginning of this section. Let's consider a control field expanded in a chopped Fourier basis that depends on N_c parameters instead of $2N_c$ parameters (as shown previously in Eq (2.1)), so that

$$\gamma^{CRAB}(t) = \sum_{i=1}^{N_c} A_i cos(\omega_i t + \theta_i) \tag{2.9}$$

where $\{A_i\}_{i=1}^{N_c}$ are the parameters the minimization now refers to, while both the frequencies ω_i and the phases θ_i are randomized, the former ones according to Eq. (2.2) and the second ones are picked with a flat distribution in $[0, 2\pi]$.
In the following graphics, the two possible optimizations are presented, both of them referring to the same randomized frequencies for each of the 30 runs of the algorithm. The total number and the range of the frequencies, the total evolution time, and the target state are the same specified at the beginning of Sec. 2.1. As expected, the minimization with respect to N_c parameters oscillates more and presents a greater infidelity mean value than the $2N_c$ parameter case, since the optimization provides better results as the parameter space dimension increases.

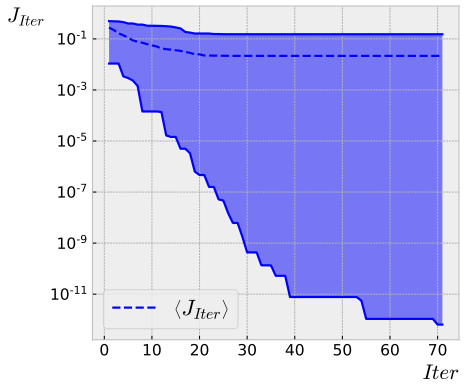

Figure 2.9: cost function (infidelity) evaluation per iteration (see caption of Fig. 2.1) corresponding to the optimization through the field expansion reported in Eq. (2.9).

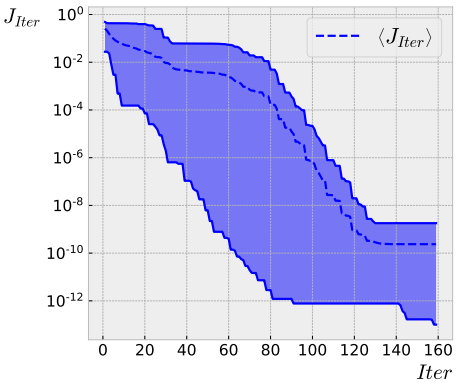

Figure 2.10: cost function (infidelity) evaluation per iteration (see caption of Fig. 2.1) corresponding to the optimization through the field expansion reported in Eq. (2.1).

2.2 Two-qubit optimization

In this section, a system made of two capacitively coupled Josephson charge qubits is considered. The Hamiltonian that drives the evolution is

$$H = H_1 + H_2 + H_{INT} \tag{2.10}$$

$$H_{1,2} = E_C \hat{\sigma}_z^{1,2} + E_J \hat{\sigma}_x^{1,2} \tag{2.11}$$

$$H_{INT} = E_{cc}(t) \hat{\sigma}_z^1 \hat{\sigma}_z^2 \tag{2.12}$$

where Eq. (2.11) is the Hamiltonian of the single qubit, Eq. (2.12) is the Hamiltonian describing the interaction between the qubits, E_c is the charging energy, E_J is the

Josephson energy and finally E_{cc} is the charging energy associated to the Coulomb interaction between the qubits.
In particular, in the following example, $\frac{E_J}{E_C} = -1$ is set, together with $\frac{E_{cc}(t)}{E_C} = \gamma(t)$. The evolution for three different target states $|\psi_G^1\rangle = |11\rangle$, $|\psi_G^2\rangle = \sum_{i,j=0}^{1} |ij\rangle$, $|\psi_G^3\rangle = \frac{1}{2}(|00\rangle + |11\rangle)$ is presented, starting from $|\psi_0\rangle = |00\rangle$ for a time evolution set equal to $T = 5\pi$ [4]. Moreover, the frequencies are picked randomly as stated in Eq. (2.2), where $r_i \in [0, 8]$.
As previously done for one-qubit system, figure 2.11 shows the cost function trend in the number of iterations of the algorithm for each different target state, with the dimension of the parameter space set to $N_c = 4$. On the other hand, Fig. 2.12 proves that the cost function esteem, calculated as mean value over 30 different runs, improves exponentially as the dimension of the parameter space increases. This is one of the main advantages CRAB algorithm provides, that is the need for just few parameters to reach the final optimization.

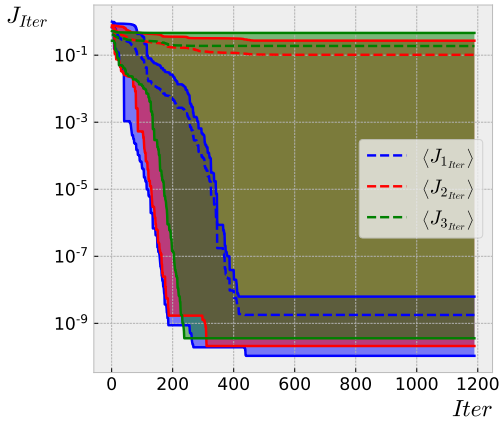

Figure 2.11: cost function (infidelity) evaluation per iteration for each target state $|\psi_G^1\rangle$ (blue), $|\psi_G^2\rangle$ (red) and $|\psi_G^3\rangle$ (green) of a two-qubit system, where the number of frequencies is fixed to $N_c = 4$; the dashed line corresponds to the mean value over 30 runs of the algorithm and the coloured space shows the maximum and minimum variation of the function along the repetitions.

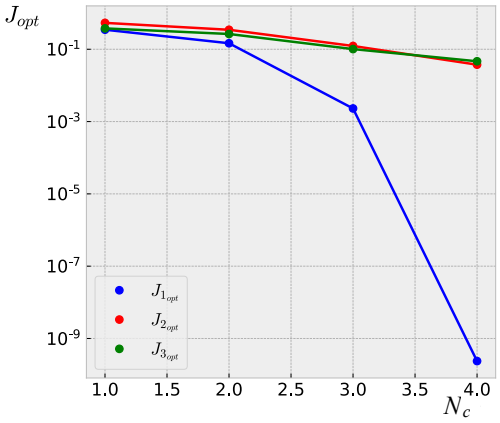

Figure 2.12: optimized cost function (infidelity) as a function of the dimension of the parameter space estimated over 30 runs of the algorithm for each target state $|\psi_G^1\rangle$ (blue), $|\psi_G^2\rangle$ (red) and $|\psi_G^3\rangle$ (green) of a two-qubit system.

Successively, a comparison between an optimization executed with randomized frequencies and non-randomized frequencies is presented. In the first case, the frequencies are chosen as reported in Eq. (2.2), while in the second case they correspond to the principal harmonics, e.g. $\omega_i = 2\pi i/T$. The optimization runs 30 times, corresponding to 30 different random frequency configurations if the randomization is applied, and 30 different values of the starting point of the initial simplex differently. The first figure 2.13 refers to the evolution towards the target state $|\psi_G^1\rangle = |11\rangle$. It is clear that the optimization made with randomized frequencies (green lines)

[4] $|00\rangle = \begin{pmatrix}1\\0\\0\\0\end{pmatrix}, |10\rangle = \begin{pmatrix}0\\1\\0\\0\end{pmatrix}, |01\rangle = \begin{pmatrix}0\\0\\1\\0\end{pmatrix}, |11\rangle = \begin{pmatrix}0\\0\\0\\1\end{pmatrix}$ is the computational basis in $\mathcal{H} = \mathbb{C}^4$.

provides better results than the other method (blue lines), as the respective cost function reaches lower values. The same conclusion can be extrapolated from the graphic 2.14 which compares the two methods by showing the trend of the infidelity in the number of parameters for each target state.

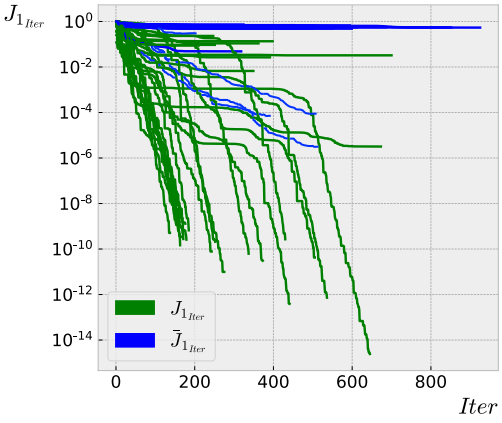

Figure 2.13: cost function (infidelity) evaluation per iteration obtained through random frequency (green) and non-random frequency (blue) optimization, corresponding to 30 different configurations of the set of random frequencies and 30 different initial points of the initial simplex respectively; the optimizations refers to the $|\psi_G^1\rangle$ target state and the number of frequencies is set equal to $N_c = 4$.

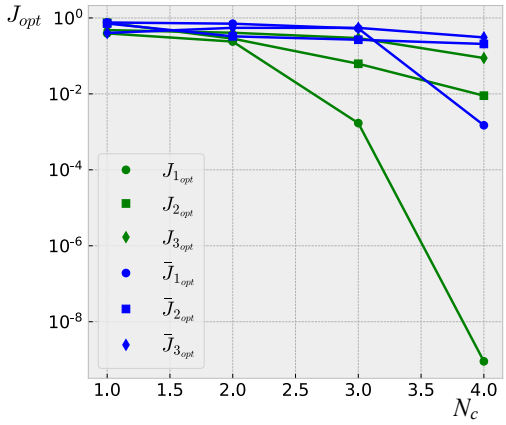

Figure 2.14: optimized cost function (infidelity) as a function of the dimension of the parameter space estimated as a mean value over 30 runs of the algorithm with randomized frequencies (green) and non-randomized frequencies (blue); the optimization for each target state $|\psi_G^1\rangle$ (circle), $|\psi_G^2\rangle$ (square) and $|\psi_G^3\rangle$ (diamond) is here presented.

Alternative: dCRAB

In the following chapter, dressed Chopped RAndom Basis algorithm is introduced as an efficient alternative to the standard method. Initially, an in-depth analysis in control landscape is presented; then, the dCRAB algorithm is applied to the same two-qubit system as previously done for the CRAB method, in order to provide a fair comparison.

3.1 Insight in control landscape

In this section, a more detailed study about what has been already mentioned in the paragraph 1.1.4 is reported. Analysis of quantum control landscapes determines the existence of optimal control solutions and their types, e.g. global or local maxima (minima) and true maxima (minima) or saddle points, but also it allows to identify necessary conditions for algorithm convergence to global maxima (minima). It has been proved that these properties are independent from the considered Hamiltonian, which makes the results of landscape analysis relevant across a wide range of controlled quantum phenomena [3].
Properties of the search space associated to Mayer-type cost functionals are particularly important in this context. In order to characterise these properties, it is convenient to express the cost functional in a form where the dynamical constraints are implicitly satisfied. Let's consider a closed quantum system with unitary evolution in $[0, T]$ and indicate by $V_T : \vec{\gamma} \to \left|\psi_{\vec{\gamma}}(T)\right\rangle$ the map from the space of control functions $\mathbb{K}$ to the space of unitary states, induced by the Schrödinger equation 1.1, so that $\left|\psi_{\vec{\gamma}}(T)\right\rangle = V_T(\vec{\gamma})$. A Mayer-type cost functional $F(\left|\psi_{\vec{\gamma}}(T)\right\rangle)$ itself describes a map F from the space of the states to the space of real-valued costs. Thus the composition of $J = F \circ V_T : \mathbb{K} \to \mathbb{R}$, is a map from the space of control functions to the space of real-valued costs. This map generates the functional $J(\vec{\gamma}) = F(V_T(\vec{\gamma}))$, defined as control landscape. This is where the definition of control landscape for state transfer problem given in section 1.1.4 comes from. The optimal control problem may then be expressed as the unconstrained search for $J_{opt} = max_{\vec{\gamma}} \{J(\vec{\gamma})\}$ [3].
As already mentioned, the topology of the control landscape determines whether local search algorithms will converge to globally optimal solutions to the control problem. So, the optimization usually leads to the critical points of the landscape, that is the points at which the first-order functional derivative of $J(\vec{\gamma})$ with respect to the control field is zero for all time

$$\frac{\delta J(\vec{\gamma})}{\delta \vec{\gamma}(t)} = 0 \quad \forall t \in [0, T] \tag{3.1}$$

and whose collection is defined as critical manifold M of the control landscape $M = \left\{\vec{\gamma} \quad | \quad \frac{\delta J(\vec{\gamma})}{\delta \vec{\gamma}(t)} = 0 \quad \forall t \in [0, T]\right\}$.
By definition and applying the chain rule, Eq. (3.1) is equivalent to

$$\delta J = \left\langle \bigtriangledown F(\psi_{\vec{\gamma}}(T)) \middle| \delta\psi_{\vec{\gamma}}(T) \right\rangle = 0 \quad \forall \vec{\gamma} \tag{3.2}$$

As a result, two constituents emerge: the fidelity gradient with respect to final state variation $\bigtriangledown F(\psi_{\vec{\gamma}}(T))/\delta\psi_{\vec{\gamma}}(T)$ and the final state variation as a function of the control variation $\delta\psi_{\vec{\gamma}}(T)/\delta\vec{\gamma}$.
As a necessary condition for a global maximum, minimum or saddle point, the gradient $\bigtriangledown F(\psi_{\vec{\gamma}}(T))/\delta\psi_{\vec{\gamma}}(T)$ has to be equal to zero [3]; particularly, if $F(\psi_{\vec{\gamma}}(T))$ corresponds to the (in)fidelity, there are no saddle points since $\bigtriangledown F = 0$ corresponds to $F = 0$ (the global minimum) or $F = 1$ (the global maximum), that is the second order variation is nonzero. Since the aim is exactly looking for a global maximum or minimum, it has to be understood under which conditions the second constituent also implies $\bigtriangledown F(\psi_{\vec{\gamma}}(T)) = 0$. Now, critical points can be classified as singular or regular ones, where regular means that for every $\left|\delta\psi_{\vec{\gamma}}(T)\right\rangle$ in the Hilbert space of the problem there is a change in the control $\delta\vec{\gamma}$ that generates it, while, on the contrary, this does not happen for singular points. So, for critical regular points, Eq. (3.2) implies that

$$\left\langle \bigtriangledown F(\psi_{\vec{\gamma}}(T))\middle|\delta\psi_{\vec{\gamma}}(T)\right\rangle = 0 \quad \forall \left|\delta\psi_{\vec{\gamma}}(T)\right\rangle \Rightarrow \bigtriangledown F = 0 \tag{3.3}$$

As a result, a regular point is not a trap, and all traps are singular points. However, as already stated in Eq. (1.1.4), numerical studies suggest that for non-constant pulses in controllable systems and in the absence of any constraints on the pulses, the landscape is free of any traps if enough process time is given, although no rigorous proof has been conducted for general systems.
Anyway, it has to be reminded that, for every realistic system, constraints on the pulses cannot be completely removed and also, in order to limit decoherence effects, it is necessary to consider short transfer time, so that the aforementioned conditions are not always fulfilled [36].

3.2 dCRAB

As already mentioned in Sec. 1.2, CRAB algorithm might converge to a non-optimal fixed point. Indeed, what stated in the previous section assumes that the control fields $\vec{\gamma}$ are general functions in L_2, so it cannot be a priori applied to functions expanded in a chopped basis: it is possible that the CRAB algorithm landscape includes points where δJ vanishes for all $\delta\vec{\gamma}$ allowed by the truncated basis expansion, but not for all variations of the entire control space. This leads to the appearance of the so called false-traps, suboptimal points defined as

$$\delta J = 0 \quad \forall\delta\vec{\gamma} \quad \wedge \quad \exists\delta\vec{\gamma} \quad | \quad \vec{\gamma} + \delta\vec{\gamma} \in L_2, \quad \delta J \neq 0 \tag{3.4}$$

As a cure, the dressed CRAB method has been introduced: when the algorithm get stuck in a false trap, the optimization is halted and the pulse information is kept, which is then resumed after employing a different set of basis functions $\{f_i(t)\}$. So, the algorithm works in an iterative way and the search per set of basis functions is referred to as a single super-iteration. Therefore, the expansion of each field of the set of control pulses $\{\gamma_j(t)\}$ results

$$\gamma^{dCRAB} = \sum_{k=1}^{N_b}\sum_{i=1}^{N_c} c^*_{k,i} f_{k,i}(t) \tag{3.5}$$

where the index i and k runs over the basis functions and the super-iterations respectively, and the asterisk $c^*_{k,i}$ indicate that those coefficients have been optimized. In particular, N_b, which set the maximum number of single super-iteration, can be fixed so that a certain threshold ϵ of the infidelity value is overcome.
Specifically, the k^{th} super-iteration optimizes the coefficients $c_{k,i}$ of

$$f_k = f_{k-1} + \sum_{i=1}^{N_c} c_{k,i} f_{k,i}(t) \tag{3.6}$$

As a consequence, the old pulse is dressed with new search directions in each super-iteration.
The mathematical reason why this method actually works is explained in the following lines. Starting from the obvious result

$$\delta J = \left\langle \bigtriangledown F(\psi_{\vec{\gamma}}(T)) \middle| \cdot \right\rangle = 2Re[\left\langle \psi_{\vec{\gamma}}(T) \middle| \psi_G \right\rangle \langle \psi_G | \cdot \rangle] \tag{3.7}$$

for a false trap, Eq. (3.7) becomes

$$\delta J = \left\langle \bigtriangledown F(\psi_{\vec{\gamma}}(T)) \middle| \cdot \right\rangle = Re[\langle \phi_T | \cdot \rangle], \quad \phi_T \neq 0 \tag{3.8}$$

Since $\delta U(T)/\delta\vec{\gamma}(t)$ can be written as $\imath U(T)U^\dagger(t)H_c U(t)$ [4], it results

$$\left| \delta\psi_{\vec{\gamma}}(T) \right\rangle = -\imath U(T) \int_0^T U^\dagger(t) H_c U(t) \left| \psi_0 \right\rangle \delta\vec{\gamma}(t) dt \tag{3.9}$$

Then, by substituting Eq. (3.8) in Eq. (3.9)

$$\delta J = \int_0^T k(t)\delta\vec{\gamma}(t)dt, \quad k(t) = -Im[\langle \phi(T) | \, U(T)U^\dagger(t)H_c U(t) \left| \psi_0 \right\rangle] \tag{3.10}$$

where $k(t)$ is continuous and necessarily $\neq 0$ since it has to satisfy Eq. (3.4). If, for example, the control pulses variations are set equal to sine or cosine functions, $\delta\gamma(t) = sin(\omega t)\delta c$ or $\delta\gamma(t) = cos(\omega t)\delta c$, then the integral in Eq. (3.10) is equal to zero only in a null set of probability measure [30]. Therefore, it results $\delta J \neq 0$ and the false trap is overcome.
In the following examples, the dCRAB algorithm is applied to the same two-qubit system presented in Sec. 2.2, and the success of an optimization is measured by a certain threshold $\epsilon = 10^{-5}$ of the infidelity value.
The figure 3.1 can be compared to the figure 2.11, since the dimension of the parameter space is set to $N_c = 4$ in both cases. In the former one, the target tolerance is achieved in only one over three evolutions presented, while in Fig. 2.11 the desired threshold is always achieved. In particular, the evolutions related to the target states $\left|\psi^2_G\right\rangle$ and $\left|\psi^3_G\right\rangle$ need two super-iterations in order to overcome ϵ.
Actually, the dCRAB algorithm can always (if there is no additional constraints) reach the target tolerance regardless of the dimension of the parameter space N_c [30]. On the contrary, false traps in the standard CRAB algorithm tend to disappear for $N_c > 2 \cdot 2^N - 2$, which is an empirical rule for unconstrained optimization where N is the number of qubits [25].

For instance, figure 2.12 shows how the infidelity esteem gets lower as N_c increases in case of the standard CRAB method, while figure 3.2, representing the same system as the previous one, shows that the the infidelity threshold $\epsilon = 10^{-5}$ is overcome for every N_c value if the dCRAB is applied. Moreover, since the CRAB cost function final evaluation strongly depends on the random frequencies, it is convenient to compute a mean value of the cost function evaluation over many different runs in order to provide a fair esteem, as it has been actually done in the previous chapter. Indeed, the frequencies randomly chosen might be more or less close to the optimal ones, so that the cost function final value results highly affected. On the contrary, thanks to his capacity to always reach the desired value, the dCRAB method does not need for such expedient, so that's why there is no mean value provided in the following graphics.
Finally, another important difference between the methods is about the computational effort required to join the optimal solution. In terms of number of function evaluation, it turns out that the computational effort highly depends on N_c for the standard CRAB, which can be problematic as the best choice of N_c is not known in advance, while this does not happen for the dCRAB algorithm. Furthermore, it has been proved that, even for the best choice of N_c, CRAB can never have a better result than dCRAB [30].

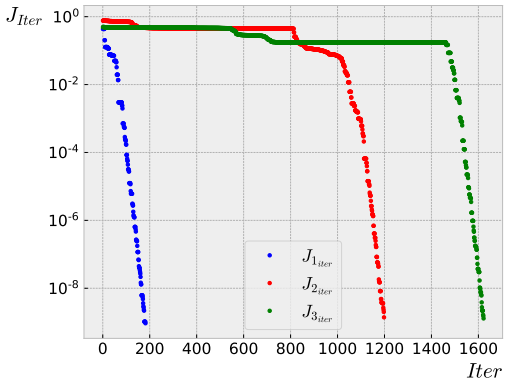

Figure 3.1: cost function (infidelity) evaluation per iteration for each target state $|\psi_G^1\rangle$ (blue), $|\psi_G^2\rangle$ (red) and $|\psi_G^3\rangle$ (green) of a two-qubit system through the dCRAB algorithm; the number of frequencies is fixed to $N_c = 4$.

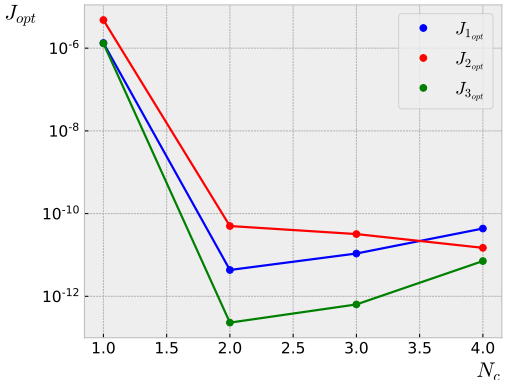

Figure 3.2: optimized cost function (infidelity) as a function of the dimension of the parameter space for each target state $|\psi_G^1\rangle$ (blue), $|\psi_G^2\rangle$ (red) and $|\psi_G^3\rangle$ (green) of a two-qubit system through the dCRAB algorithm; the infidelity esteems for every N_c value are below the fixed threshold $\epsilon = 10^{-5}$.

Conclusion

In this thesis, properties and effectiveness of the CRAB algorithm are presented. First of all, the method was applied to a system made of one qubit. This was done in several ways so as to show properties the algorithm holds: different forms of the Fourier decomposition were used, stressing that the choice of the function basis as well as the optimization parameters is arbitrary; moreover, three different ways of imposing constraints on the pulse amplitude were shown. Successively, the algorithm was applied to a more complex system, that is two capacitively coupled Josephson charge qubits. Here, two considerations were made: an exponential dependence of the cost function on the number of optimization parameters was presented, underling the fast convergence of the algorithm; a comparison between a randomized and non-randomized frequency optimization was reported, proving that the former one actually provides lower cost function evaluations, since randomizing the frequencies of the field, expanded in a truncated basis, enlarges the search volume for the optimal solution in terms of the function space. Finally, the dressed CRAB (dCRAB) method was shown as a solution to avoid false traps where the algorithm might get stuck even in case of unconstrained pulse, due to the restriction of the search basis to N_c dimensions given by the CRAB expansion. This version of the algorithm successfully achieves the target cost function value regardless of the number of parameters in the field expansion, so it consist of a valid alternative to standard CRAB algorithm. To conclude, the main features of the Chopped RAndom Basis algorithm were presented, such as efficiency in the use of just few optimization parameters, suitability in the application to different systems as well as in the definition of the cost function and high probability of success in terms of achieving a target threshold for the cost function esteem.

Bibliography

[1] Antonio Acín et al. "The European quantum technologies roadmap". In: *arXiv preprint arXiv:1712.03773* (2017).

[2] Francesca Albertini and Domenico D'Alessandro. "Notions of controllability for bilinear multilevel quantum systems". In: *IEEE Transactions on Automatic Control* 48.8 (2003), pp. 1399–1403.

[3] Constantin Brif, Raj Chakrabarti, and Herschel Rabitz. "Control of quantum phenomena: past, present and future". In: *New Journal of Physics* 12.7 (2010), p. 75008. DOI: 10.1088/1367-2630/12/7/075008. URL: https://doi.org/10.1088{\%}2F1367-2630{\%}2F12{\%}2F7{\%}2F075008.

[4] Constantin Brif et al. *Searching for quantum optimal controls in the presence of singular critical points.* Tech. rep. Sandia National Lab.(SNL-CA), Livermore, CA (United States), 2014.

[5] Tommaso Caneva, Tommaso Calarco, and Simone Montangero. "Chopped random-basis quantum optimization". In: *Physical Review A* 84.2 (2011), p. 022326.

[6] Tommaso Caneva, Tommaso Calarco, and Simone Montangero. "Entanglement-storage units". In: *New Journal of Physics* 14.9 (2012), p. 093041.

[7] Tommaso Caneva et al. "Optimal control at the quantum speed limit". In: *Physical review letters* 103.24 (2009), p. 240501.

[8] Domenico d'Alessandro. *Introduction to quantum control and dynamics.* Chapman and Hall/CRC, 2007.

[9] Pierre de Fouquieres and Sophie G Schirmer. "Quantum control landscapes: A closer look". In: *arXiv preprint arXiv:1004.3492* (2010).

[10] Florian Frank et al. "Autonomous calibration of single spin qubit operations". In: *npj Quantum Information* 3.1 (2017), pp. 1–5.

[11] Fuchang Gao and Lixing Han. "Implementing the Nelder-Mead simplex algorithm with adaptive parameters". In: *Computational Optimization and Applications* 51.1 (2012), pp. 259–277.

[12] Steffen J Glaser et al. "Training Schrödinger's cat: quantum optimal control". In: *The European Physical Journal D* 69.12 (2015), p. 279.

[13] Michael H Goerz et al. "Krotov: A Python implementation of Krotov's method for quantum optimal control". In: *methods* 15 (2019), p. 1.

[14] Robert Heck et al. "Remote optimization of an ultracold atoms experiment by experts and citizen scientists". In: *Proceedings of the National Academy of Sciences* 115.48 (2018), E11231–E11237.

[15] Navin Khaneja, Roger Brockett, and Steffen J Glaser. "Time optimal control in spin systems". In: *Physical Review A* 63.3 (2001), p. 032308.

[16] Navin Khaneja et al. "Optimal control of coupled spin dynamics: design of NMR pulse sequences by gradient ascent algorithms". In: *Journal of magnetic resonance* 172.2 (2005), pp. 296–305.

[17] Vadim Krotov. *Global methods in optimal control theory.* Vol. 195. CRC Press, 1995.

[18] Davide La Torre et al. "Optimal control: theory and application to science, engineering, and social sciences". In: *Abstract and Applied Analysis*. Vol. 2015. Hindawi. 2015.

[19] Jeffrey C Lagarias et al. "Convergence properties of the Nelder–Mead simplex method in low dimensions". In: *SIAM Journal on optimization* 9.1 (1998), pp. 112–147.

[20] S Lloyd and S Montangero. "Information theoretical analysis of quantum optimal control". In: *Physical review letters* 113.1 (2014), p. 010502.

[21] Dawei Lu et al. "Enhancing quantum control by bootstrapping a quantum processor of 12 qubits". In: *npj Quantum Information* 3.1 (2017), pp. 1–7.

[22] Shai Machnes et al. "Tunable, flexible, and efficient optimization of control pulses for practical qubits". In: *Physical review letters* 120.15 (2018), p. 150401.

[23] L Mandelstam and IG Tamm. "The uncertainty relation between energy and time in non-relativistic quantum mechanics". In: *Selected Papers*. Springer, 1991, pp. 115–123.

[24] Norman Margolus and Lev B Levitin. "The maximum speed of dynamical evolution". In: *Physica D: Nonlinear Phenomena* 120.1-2 (1998), pp. 188–195.

[25] Katharine W Moore and Herschel Rabitz. "Exploring constrained quantum control landscapes". In: *The Journal of chemical physics* 137.13 (2012), p. 134113.

[26] Oleg Vasilevich Morzhin and Alexander Nikolaevich Pechen. "Krotov method for optimal control of closed quantum systems". In: *Russian Mathematical Surveys* 74.5 (2019), p. 851.

[27] J. A. Nelder and R. Mead. "A Simplex Method for Function Minimization". In: *The Computer Journal* 7.4 (Jan. 1965), pp. 308–313. ISSN: 0010-4620. DOI: 10.1093/comjnl/7.4.308. URL: https://doi.org/10.1093/comjnl/7.4.308.

[28] Ahmed Omran et al. "Generation and manipulation of Schrödinger cat states in Rydberg atom arrays". In: *Science* 365.6453 (2019), pp. 570–574.

[29] Alexander N Pechen and David J Tannor. "Are there traps in quantum control landscapes?" In: *Physical review letters* 106.12 (2011), p. 120402.

[30] Niklas Rach et al. "Dressing the chopped-random-basis optimization: A bandwidth-limited access to the trap-free landscape". In: *Physical Review A* 92.6 (2015), p. 062343.

[31] SG Schirmer, AI Solomon, and JV Leahy. "Degrees of controllability for quantum systems and application to atomic systems". In: *Journal of Physics A: Mathematical and General* 35.18 (2002), p. 4125.

[32] Mary C Seiler and Fritz A Seiler. "Numerical recipes in C: the art of scientific computing". In: *Risk Analysis* 9.3 (1989), pp. 415–416.

[33] Moshe Shapiro and Paul Brumer. "Principles of the quantum control of molecular processes". In: *Principles of the Quantum Control of Molecular Processes, by Moshe Shapiro, Paul Brumer, pp. 250. ISBN 0-471-24184-9. Wiley-VCH, February 2003.* (2003), p. 250.

[34] JJWH Sørensen et al. "Quantum optimal control in a chopped basis: Applications in control of Bose-Einstein condensates". In: *Physical Review A* 98.2 (2018), p. 022119.

[35] Zdeněk Tošner et al. "Optimal control in NMR spectroscopy: Numerical implementation in SIMPSON". In: *Journal of Magnetic Resonance* 197.2 (2009), pp. 120–134.

[36] Jonathan Zoller. "Optimal quantum engineering". PhD thesis. Universität Ulm, 2018.